

Integrated Decision-Making and Control for Urban Autonomous Driving with Traffic Rules Compliance

Haichao Liu, Kai Chen, Yulin Li, Zhenmin Huang, Jianghua Duan, and Jun Ma

Abstract—In urban driving scenarios, autonomous vehicles are expected to conform to traffic rules covering traffic lights, traversable and non-traversable traffic lines, etc. In this article, we propose an optimization-based integrated decision-making and control scheme for urban autonomous driving. Inherently, to ensure the compliance with traffic rules, an innovative design of potential functions (PFs) is presented to characterize various traffic rules that are commonly encountered in urban driving scenarios, and these PFs are further incorporated as part of the model predictive control (MPC) formulation. In this sense, it circumvents the necessity of typical hand-crafted rule design, and high-level decision-making is attained implicitly along with control as an integrated architecture, facilitating flexible maneuvers with safety guarantees. As demonstrated from a series of simulations in CARLA, it is noteworthy that the proposed framework admits real-time performance and high generalizability.

I. INTRODUCTION

A. Background and Related Works

Recent developments in the automobile industry prompt the emergence of autonomous vehicles, which enhance the safety and efficiency of transportation. Typically, autonomous vehicles are equipped with multiple sensors to gather information about the surrounding traffic conditions, from which the driving strategies are derived accordingly [1]. However, ego-vehicle perceptions are subject to limitations in range and accuracy, which would be downgraded due to nonideal external conditions, such as harsh weather and darkening ambient light. To compensate for the deficiencies of ego-vehicle perceptions, the vehicle to everything (V2X) technique has been extensively studied [2]. Notably, V2X facilitates real-time communications between vehicles and road facilities, which increases the reliability of gathered information. In this sense, the V2X-based perception lays a solid foundation for autonomous driving systems.

Despite the advancements in perceptions, a series of problems remain primarily unsolved in developing effective decision-making and control schemes, especially in various

complicated urban driving scenarios. To tackle these problems, hierarchical frameworks are intensively researched, which generally split the decision-making and control processes into consecutive modules. In [3], a motion planning system covering multi-lane and single-lane autonomous driving is proposed, which admits a high-level multi-lane strategy to handle the lane change and a low-level inner-lane strategy to perform iterative path and speed optimization, respectively. In [4], a finite state machine (FSM) based controller is described and applied to highway driving scenarios. Moreover, a goal recognition system based on the decision tree is introduced in [5] to perform decision-making and provide interpretability, such that safety can be formally verified. Generally, real-world trajectory data of vehicles are required to train the decision tree. Hence, hierarchical frameworks typically involve man-made heuristic rules with a limited number [6]. As a consequence, its generalizability to different urban traffic scenarios is limited, and various corner cases cannot be catered to appropriately.

Significant efforts have been dedicated to dealing with the aforementioned drawbacks that are typically encountered in hierarchical frameworks. In particular, with the rapid development of data science and artificial intelligence, learning-based methods are investigated to circumvent the necessities of man-made heuristic rules. In [7], [8], [9], reinforcement learning is adopted to address difficult urban traffic scenarios without the use of hand-crafted rules. However, the lack of interpretability hinders their wide application in real-world applications. Another popular category is integrated optimization frameworks, which also remove heuristic rules but provide good interpretability [10]. Integrated optimization frameworks generally formulate the decision-making process and the low-level control problem as an integrated optimization problem, such that the overall optimal strategies can be obtained. In [11], [12], mixed-integer programming (MIP) is adopted to handle the decision-making part and obtain the discretized decision variables. However, MIP is generally considered to be rather time-consuming, which defies the real-time requirements of control for autonomous vehicles. For the improvement of computation efficiency, the artificial potential field (APF) can be suitably adopted, which integrates various forms of potential functions into the optimization goal to realize simultaneous decision-making and control, exhibiting both flexibility in problem formulation and high computation efficiency. Remarkably, a model predictive control scheme incorporating APF is proposed in [13], where both the road and vehicles are modeled as non-crossable obstacles, and collision avoidance with surrounding

Haichao Liu, Kai Chen, and Jun Ma are with the Robotics and Autonomous Systems Thrust, The Hong Kong University of Science and Technology (Guangzhou), Guangzhou, China (e-mail: hliu369@connect.hkust-gz.edu.cn; kchen916@connect.hkust-gz.edu.cn; jun.ma@ust.hk).

Yulin Li and Zhenmin Huang are with the Department of Electronic and Computer Engineering, The Hong Kong University of Science and Technology, Hong Kong SAR, China (e-mail: yline@connect.ust.hk; zhuangdf@connect.ust.hk).

Jianghua Duan is with the Department of Mechanical and Aerospace Engineering, The Hong Kong University of Science and Technology, Hong Kong SAR, China (e-mail: jhduan@ust.hk).

Haichao Liu and Kai Chen contributed equally to this work. All correspondence should be sent to Jun Ma.

vehicles is successfully performed without violating the road constraints in the straight-line driving test scenario. In [14], APF is introduced into emergency avoidance tasks, and the minimum collision cost is obtained when the collision cannot be avoided. In [15], the lane-change maneuver is realized by applying an attractive force generated by the goal point. Nonetheless, these works only present relatively simple test and verification scenarios and are hard to deploy in real urban driving tasks with high complexity. Another common problem is that traffic lights are not typically considered in the proposed APFs. In [16], the red traffic light state is treated as a hard constraint, which causes the vehicle to brake suddenly when it is close to the intersection; and apparently, this affects the comfort of passengers and driving safety. Therefore, it remains an interesting problem to propose specific strategies to cater to traffic lights based on an effective design of the potential function (PF).

B. Contributions

This paper proposes an interpretable and computationally efficient optimization-based autonomous driving framework that realizes the integration of decision-making and control with a global navigation path. The contributions are as follows:

- An optimization-based integrated decision-making and control scheme is proposed, which renders real-time performance in urban autonomous driving. Particularly, as encoded by the APF (which is incorporated in the objective function of MPC), high-level decision-making is attained implicitly along with control.
- An innovative design of PFs is proposed to characterize the traffic rules that are commonly encountered in urban driving scenarios, such that the compliance with traffic rules is ensured without the necessity of typical hand-crafted rule design.
- The proposed framework admits high generalizability due to the integrated decision-making and control scheme design, and thorough simulations are performed in CARLA simulator towards a series of randomly generated scenarios.
- An open-source implementation of the proposed integrated decision-making and control framework is released.

II. V2X- BASED AUTONOMOUS DRIVING FRAMEWORK

In order to integrate decision-making and control processes, we need to establish an autonomous driving framework based on V2X communication. The proposed autonomous driving framework contains three modules: (a) global path planning and smoothing, (b) V2X information collection, and (c) dynamic decision-making and control. The framework can fully leverage environmental information, achieve efficient obstacle avoidance, and strongly adapt to traffic rules, while path or trajectory re-planning is not required during the whole process of autonomous driving. Additionally, this framework can be executed lightly on computer equipment with low configuration.

A. Initial Path Planning and Smoothing

In the path search process, waypoints are sampled along the center line of lanes with equal intervals in the Open-DRIVE map. To construct the connectivity graph, each waypoint is connected with its direct predecessor and successor on the same lane and its adjacent waypoints on the left or right lane. Therefore, for any starting point, A* search can be performed on the connectivity graph to obtain the shortest path leading to the target destination. Note that the above simplification on the path can essentially speed up the search in global path planning and improve the continuity of the searched path. After the global reference waypoints are obtained, the local reference waypoints can be determined through spline interpolation. The interpolation considers the current speed of the ego vehicle (EV), thus ensuring that the generated waypoints are trackable over time. Moreover, since we use spline curves, the trajectories generated by the interpolation are smooth.

B. Information Collection from V2X Communication

Through V2X communication, we can accurately perceive the current states of surrounding vehicles, different lane markings, and traffic lights, providing detailed reference information for obstacle avoidance and traffic rule compliance. Since this work focuses on the design of the integrated decision-making and control scheme such that obstacles can be effectively avoided under the premise of traffic rule compliance, we ignore the delay of V2X communication and assume that the V2X communication is stable and reliable in all scenarios. Specifically, in order to avoid obstacles, it is necessary to obtain the position and velocity information of vehicles within a certain range around the EV. In order to obey the traffic rules, it is necessary to obtain the type of lane markings on both sides where the ego vehicle is currently located, as well as the current state of the traffic lights near the EV. To the best of our knowledge, existing works on model-based decision-making and control schemes hardly consider traffic light constraints.

C. Dynamic Decision-Making and Control

In urban driving scenarios, the environment around the EV is dynamically changing with high complexity. Therefore, the appropriate formulation and efficient solving of the decision and control problem are the basis that guarantees the safety of autonomous vehicles. This optimization problem aims to track the waypoints obtained by spline interpolation in Section II-A. The constraints mainly include the dynamics model of the vehicle, the boundary of vehicle control, the surrounding vehicle avoidance, the traffic rule constraints in terms of lane markings and traffic lights, etc. Note that the traffic rule constraints are formulated as PFs to guide the EV to drive to keep away from the risk fields.

III. OPTIMIZATION-BASED INTEGRATED DECISION-MAKING AND CONTROL SCHEME

With a variety of PFs, the proposed integrated decision-making and control scheme can implicitly generate decision-making commands (such as overtaking or following) in

a receding horizon manner. It receives the environmental perception and global path information from the upstream modules; and then it makes implicit and continuous decisions and outputs the acceleration and steering angle of the EV.

A. Vehicle Dynamics Model

Because the speed of autonomous vehicles varies widely under urban driving scenarios, this paper uses the nonlinear dynamics model proposed by [17] to represent the vehicle dynamics precisely. The model exhibits good numerical stability and high fidelity in the scene of frequent acceleration and deceleration as is typically observed in urban driving tasks. The state vector of the dynamics model is $\mathbf{x} = [\mathbf{p}, \phi, \mathbf{v}, \omega]^T$ where $\mathbf{p} = [p_x, p_y]^T$ is the vehicle position in the global Cartesian frame, and $\mathbf{v} = [v_x, v_y]^T$ is the velocity in the EV frame. Besides, ϕ is the heading angle referring to the global Cartesian frame, and ω is the yaw rate. The control input of the system is $\mathbf{u} = [a, \delta]^T$, where a and δ represent the acceleration and steering angle, respectively. Notice that the control input δ cannot change suddenly with infinite angular acceleration due to the existence of inertia. Hence, we need to add the smoothness cost to the optimization problem for decision-making and control, which can also improve passengers' comfort. We utilize the discrete model derived from backward Euler method:

$$\mathbf{x}_{\tau+1} = f(\mathbf{x}_\tau, \mathbf{u}_\tau)$$

$$= \begin{bmatrix} p_x(\tau) + T_s (v_x(\tau) \cos \varphi(\tau) - v_y(\tau) \sin \varphi(\tau)) \\ p_y(\tau) + T_s (v_y(\tau) \cos \varphi(\tau) + v_x(\tau) \sin \varphi(\tau)) \\ \varphi(\tau) + T_s \omega(\tau) \\ v_x(\tau) + T_s a(\tau) \\ \frac{mv_x(\tau)v_y(\tau) + T_s L_k \omega(\tau) - T_s k_f \delta(\tau) v_x(\tau) - T_s m v_x(\tau)^2 \omega(\tau)}{mv_x(\tau) - T_s (k_f + k_r)} \\ \frac{I_z v_x(\tau) \omega(\tau) + T_s L_k v_y(\tau) - T_s l_f k_f \delta(\tau) v_x(\tau)}{I_z v_x(\tau) - T_s (l_f^2 k_f + l_r^2 k_r)} \end{bmatrix}, \quad (1)$$

where we denote m as the vehicle mass, l_f and l_r as the distance from the mass center to the front and rear axle, k_f and k_r as the cornering stiffness of the front and rear wheels, and I_z as the inertia polar moment. For simplicity, we define $L_k = l_f k_f - l_r k_r$. Table I lists the parameter settings in the above model.

B. Potential Functions Design

Typically, the APF is centered on the obstacle or the goal, which emits a repulsive or attractive force field to the environment, so that the system is driven to the destination without collisions. In this paper, the repulsive PF for surrounding vehicles, the repulsive PF for non-traversable lane markings, and the attractive PF for the centerline of lanes are designed. Unlike the traditional APF method, where the target position is set as a gravitational field [18], this paper employs several novel quadratic penalty terms for collision avoidance and traffic rules compliance. Therefore, the potential field in the integrated decision and control module is characterized as

$$F(\mathbf{p}_{\text{env}}, \mathbf{x}) = \sum_i F_{\text{NR}_i} + \sum_j F_{\text{CR}_j} + \sum_k F_{\text{V}_k} + \sum_q F_{\text{TL}_q}, \quad (2)$$

TABLE I
PARAMETER SETTINGS OF THE VEHICLE MODEL

Notation	Value	Unit	Notation	Value	Unit
k_f	-128916	N/rad	l_r	1.85	m
k_r	-85944	N/rad	m	1412	kg
l_f	1.06	m	I_z	1536.7	kg · m ²

where i, j, k , and q denote the indices of non-traversable lane markings, traversable lane markings, surrounding vehicles, and dynamic traffic lights, respectively. To simplify the PF design, we classify various types of lane markings on the road into two categories: traversable lane markings represented by broken lines and non-traversable lane markings represented by solid lines.

The lateral distance from the EV to the lane marking is an essential value to determine the PF force. We define the road centerline state vector as $\mathbf{p}_i = [p_{x,i}, p_{y,i}, \beta_i]^T$, where the first two items $p_{x,i}$ and $p_{y,i}$ represent the position of the current road centerline in global Cartesian frame, and the last item β_i is the tangential angle of the current road. Therefore, the lateral position of the lane marking is given as

$$s_R(\mathbf{x}, \mathbf{p}_i) = \begin{cases} \left(p_y^{\text{ev}}(\mathbf{p}_i) + \frac{w_R}{2} \right) - y^{\text{ev}}(\mathbf{x}, \mathbf{p}_i) & \text{left} \\ y^{\text{ev}}(\mathbf{x}, \mathbf{p}_i) - \left(p_y^{\text{ev}}(\mathbf{p}_i) - \frac{w_R}{2} \right) & \text{right} \end{cases} \quad (3)$$

where "left" and "right" indicate the lane marking on the left or right side of the vehicle, w_R is the lane width, p_y^{ev} and y^{ev} are the lateral positions of the lane centerline and the EV in the proposed heading angle-parallelled (HAP) frame, in which the orientation of the road is parallelled with the x -axis. Thus, the above lateral positions in the HAP frame are

$$p_y^{\text{ev}}(\mathbf{p}_i) = p_{x,i} \sin(\beta_i) + p_{y,i} \cos(\beta_i), \quad (4)$$

$$y^{\text{ev}}(\mathbf{x}, \mathbf{p}_i) = p_x \sin(\beta_i) + p_y \cos(\beta_i). \quad (5)$$

Then the PFs for lane markings can be effectively expressed as follows.

1) *Non-Traversable Lane Markings*: To comply with traffic rules, vehicles must not traverse a solid lane marking. Especially when the lane marking is next to curbstones or a sidewalk, crossing it results in potential danger. Therefore, when the distance between the EV and the surrounding lane markings decreases to a certain extent, the designed PF should give a repulsive force that increases rapidly with decreasing distance to urge the EV to steer away immediately. Based on the inverse proportional function and power function, we designed the following PF for the i th non-traversable lane marking:

$$F_{\text{NR}_i} = \begin{cases} m_s & s_{R_i} \leq 0.1 \\ \frac{a_{\text{NR}}}{s_{R_i}(\mathbf{x}, \mathbf{p}_i)^{b_{\text{NR}}}} - e_s & 0.1 < s_{R_i} < 1.5 \\ 0 & s_{R_i} \geq 1.5 \end{cases}, \quad (6)$$

where a_{NR} and b_{NR} are the intensity and shape parameters that control the strength of the repulsive force and the

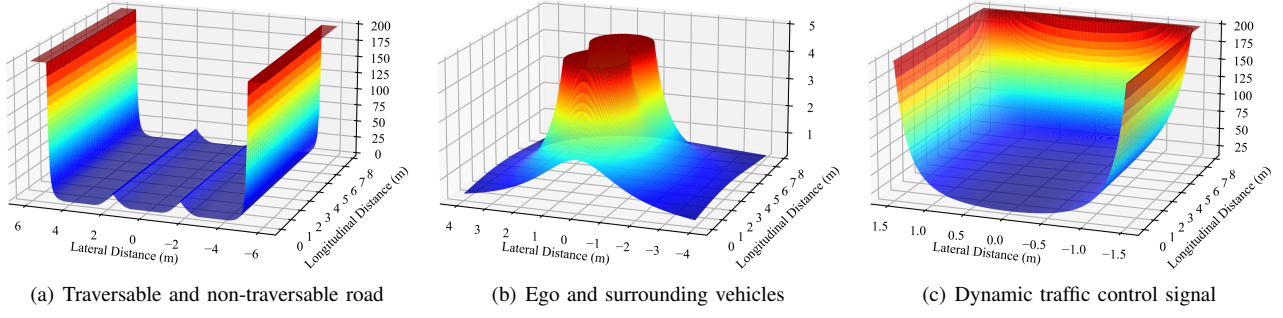


Fig. 1. The designed potential functions for traversable and non-traversable lane markings, surrounding vehicles, and red traffic light signals. (a) The potential field is summarized by two traversable and two non-traversable lane markings, which construct a three-lane road structure. The lateral position of non-traversable markers and traversable markers are $[5.25, -5.25]$ m and $[1.75, -1.75]$ m, respectively. (b) The PF obtained by wrapping a vehicle using two circles, where the parameters of the PF are set as $[p_{k,x}, p_{k,y}] = [3.0, 0]$ m, $a_V = 5.0$, and $r_V = 1.2$ m. (c) The PF of the red traffic light, where the parameters of the PF are set as $p_y^{ev} = 8.0$ m, $a_{TL_1} = 20$, and $a_{TL_2} = 40$.

effective range of the PF. The smooth parameters

$$e_s = \frac{a_{NR}}{1.5b_{NR}}, \quad m_s = \frac{a_{NR}}{0.1b_{NR}} - e_s$$

guarantee the continuity of the PF value when s_{R_i} switches to another condition. The 3D shape of the designed non-traversable lane marking's PF is illustrated on both sides of Fig. 1(a), where $a_{NR} = 100$ and $b_{NR} = 2.0$.

2) *Traversable Lane Markings*: In the process of overtaking and lane changing, it is necessary to traverse the broken lane marking on the road. When the reference lane of the EV is blocked from ahead by other traffic participants, the EV needs to switch to an adjacent lane and keeping driving until the reference lane is free. When EV is driving on a lane that is not the reference one, designing a PF that keeps the EV driving along the centerline is necessary, as otherwise the EV will be attracted to the side of the current lane due to the attractive force of the reference lane. Thus, the PF of the j th traversable lane marking is designed as follows:

$$F_{CR_j} = \begin{cases} a_{CR}(s_R(\mathbf{x}, \mathbf{p}_j) - b_{CR})^2 & s_{R_j} < b_{CR} \\ 0 & s_{R_j} \geq b_{CR} \end{cases}, \quad (7)$$

where a_{CR} is the intensity parameter and b_{CR} is the effective range of the repulsive force from the lane marking. Such PF repulses the EV away from the lane marking and forces it to stay around the lane center. The 3D shape of the traversable lane marking PF is shown in the middle area of Fig. 1(a), where the parameters are $a_{CR} = 20$ and $b_{CR} = 1.0$.

3) *Surrounding Vehicles*: The main traffic participants on the road are vehicles and pedestrians, both of which are strictly prohibited to collide into. We approximate each on-road vehicle with two identical circles aligned in the longitudinal direction that covers the entire vehicle. In order to avoid surrounding vehicles smoothly and quickly, we design the following PF:

$$F_{V_k} = \sum_{o=1}^2 \frac{a_V}{((p_x - p_{k,o,x})^2 + (p_y - p_{k,o,y})^2)^{b_V}}, \quad (8)$$

where a_V and b_V are the intensity and shape parameters, which control the strength of the repulsive force and the

effective range of this PF. As the vehicle is represented by two circles, we must calculate the circles' positions and sum their force to formulate the integrated PF. The position vector $[p_{k,o,x}, p_{k,o,y}]^T$ denotes position of the o th circle of the k th surrounding vehicle, and we have

$$\begin{bmatrix} p_{k,o,x} \\ p_{k,o,y} \end{bmatrix} = \begin{bmatrix} 1 & 0 \\ 0 & 1 \end{bmatrix} \begin{bmatrix} p_{k,x} \\ p_{k,y} \end{bmatrix} \pm \begin{bmatrix} \cos \beta_i \\ \sin \beta_i \end{bmatrix} r_V, \quad (9)$$

where the common radius of the circles is $r_V = 1.2$ and $o = \{0, 1\}$ indicates whether the circle is front or rear. Without loss of generality, (8) can also be used to avoid collisions with pedestrians by using only one circle centered at the pedestrian's head, but V2X communication cannot directly get the pedestrian's state on the road. Thus, pedestrians are not considered in our urban driving tests. Fig. 1(b) illustrates the potential field of a vehicle in front of the EV, where the parameters are set as $[p_{k,x}, p_{k,y}] = [3.0, 0]$ m, $a_V = 5.0$, and $r_V = 1.2$ m.

4) *Traffic Lights*: In addition to obeying the rules of lane markings, vehicles must also obey the command of traffic lights. This paper proposes a novel PF for traffic lights, which can restrict the lateral and longitudinal positions of the EV simultaneously. The PF applies repulsive forces in three directions to the ego vehicle without changing its original reference trajectory. In particular, the PF is designed as

$$F_{TL} = c_{TL} \left(\frac{a_{TL_1}}{d_x^{ev}} + \frac{a_{TL_2}}{d_{y,l}^{ev}} + \frac{a_{TL_2}}{d_{y,r}^{ev}} \right), \quad (10)$$

where c_{TL} is an indicator of the state of the traffic light, which equals to 0 is the traffic light is *green* and 1.0 otherwise. Besides, a_{TL_1} and a_{TL_2} are intensity parameters in the longitudinal and lateral orientations, respectively, and d_x^{ev} is the longitudinal distance from EV to the stop line. Moreover, $d_{y,l}^{ev}$, $d_{y,r}^{ev}$ are the distance of the EV to the left and right lane markings, respectively, which can be calculated by (3) as well.

C. Integrated Decision-Making and Control: Optimization Problem Formulation

This section formulates the decision-making and control scheme, which leverages the MPC to solve an optimal control

problem (OCP) in the receding horizon manner. The cost function is formulated as

$$J(\mathbf{x}, \mathbf{u}, \mathbf{p}_{\text{env}}) = \sum_{\tau=1}^N \|\mathbf{x}_{\text{ref},\tau} - \mathbf{x}_\tau\|_{\mathbf{Q}}^2 + \sum_{\tau=1}^N \|\mathbf{u}_\tau\|_{\mathbf{R}}^2 + \sum_{\tau=2}^N \|\mathbf{u}_\tau - \mathbf{u}_{\tau-1}\|_{\mathbf{R}_d}^2 + F(\mathbf{p}_{\text{env}}, \mathbf{x}), \quad (11)$$

where N is the length of the receding horizon, $\mathbf{x}_{\text{ref},\tau} \in \mathbb{R}^6$ is the reference trajectory point generated by spline interpolation based on the global path at the time step τ . In (11), $\mathbf{Q} \in \mathbb{R}^{6 \times 6}$, $\mathbf{R} \in \mathbb{R}^{2 \times 2}$, $\mathbf{R}_d \in \mathbb{R}^{2 \times 2}$ are positive semi-definite diagonal weighting matrices for penalizing reference tracking, energy saving, and passenger comfort, respectively. $F(\mathbf{p}_{\text{env}}, \mathbf{x})$ is the artificial potential field generated according to the V2X information, as described in (2).

Therefore, the OCP is constructed as:

$$\begin{aligned} \min_{\mathbf{x}, \mathbf{u}} \quad & J(\mathbf{x}, \mathbf{u}, \mathbf{p}_{\text{env}}) \\ \text{s.t.} \quad & \mathbf{x}_{\tau+1} = f(\mathbf{x}_\tau, \mathbf{u}_\tau), \forall \tau \in \{1, 2, \dots, N\} \\ & -\mathbf{u}_{\min} \preceq \mathbf{u}_\tau \preceq \mathbf{u}_{\max}, \forall \tau \in \{1, 2, \dots, N\} \\ & -\mathbf{x}_{\min} \preceq \mathbf{x}_\tau \preceq \mathbf{x}_{\max}, \forall \tau \in \{1, 2, \dots, N\} \\ & m \preceq d_{\tau,n,ij}, \forall \tau \in \{1, 2, \dots, N\}, \\ & \forall n \in \{1, 2, \dots, S\}, \forall i, j \in \{1, 2\}. \end{aligned} \quad (12)$$

Note that the first constraint represents the vehicle dynamics (1). The second and third constraints indicate the restriction on the control inputs and system state variables, which are based on the physical properties of the selected vehicle model. The last constraint is the obstacle avoidance constraint with surrounding vehicles, where $d_{\tau,n,ij}$ denotes the distance from the ego vehicle to surrounding vehicles at time step τ . As the vehicle is represented by two circles to avoid collisions, the distance between the i th circle of the EV and the j th circle of the n th surrounding vehicle should be calculated at each optimization step.

Problem (12) is reformulated to a nonlinear programming (NLP) problem. Direct multiple shooting method is used to solve (12) numerically, in which we treat the states at shooting nodes as decision variables and improves convergence by lifting the NLP problem to a higher dimension. Then we solve the NLP problem using the Interior Point Optimizer (IPOPT) with CasADi [19] in Python.

IV. SIMULATION RESULTS

In this section, we comprehensively evaluate the proposed integrated decision-making and control framework towards three different representative urban driving scenarios in CARLA [20]. In the simulation environment, we control the EV to follow the pre-computed global path under highly dynamic city roads, where the spawn positions and trajectories of other vehicles are generated randomly using the embedded "autopilot" mode. Except for ensuring collision-free with surrounding vehicles, common traffic elements like lane markings and traffic lights are considered as PFs. To further demonstrate the practicality and effectiveness in traffic rule compliance, the impacts of the designed PFs

on generating safe and flexible maneuvers are discussed in detail.

We implement the proposed algorithm in Ubuntu 20.04 LTS, and execute the simulation using AMD Ryzen 5600G CPU and NVIDIA RTX 3060 GPU with 16 GB RAM and 12 GB Graphic Memory. The code of the proposed integrated decision-making and control scheme and the autonomous driving framework constructed in CARLA simulator are available at <https://github.com/HKUST-JM/Optimization-based-IDMC-CARLA.git>.

A. Simulation Scenarios

1) *Scenario 1: Roundabout Driving*: In the roundabout scenario, the EV is going to enter the roundabout from the east entrance, and leave at the opposite exit. Typically, the heavy traffic flow renders great difficulties for this task. Moreover, the frequent and unpredictable lane-changing behavior of other vehicles makes the driving task even more challenging.

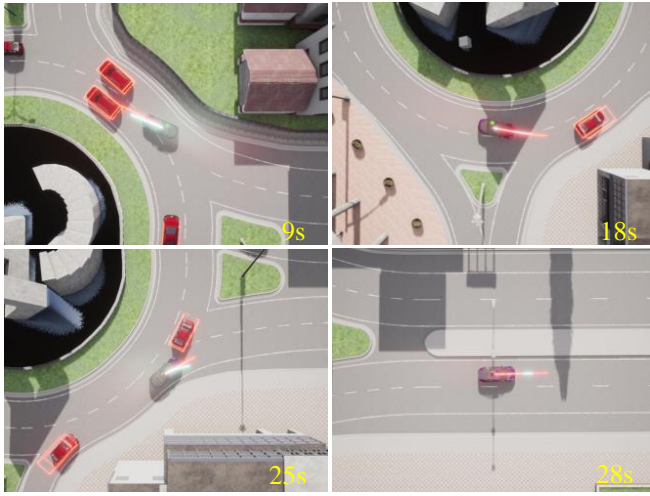
2) *Scenario 2: Multi-Lane Adaptive Cruise Control*: In this scenario, the EV aims to follow the centerline of the current lane at a given speed as much as possible while keeping a safe distance from the leading vehicle until reaching the terminal state. It is pertinent to note that, apart from maintaining a safe distance from surrounding vehicles, traversable and non-traversable lane markings should also be considered in this task.

3) *Scenario 3: Crossroad Driving*: To get through the crossroad safely, the EV needs to quickly response to the state change of the traffic light. In this task, the global path leads the vehicle to a left turn at the dense crossroad where the traffic light is about to turn red as the EV approaches. Meanwhile, the non-traversable lane markings constraints cannot be violated during the turning process.

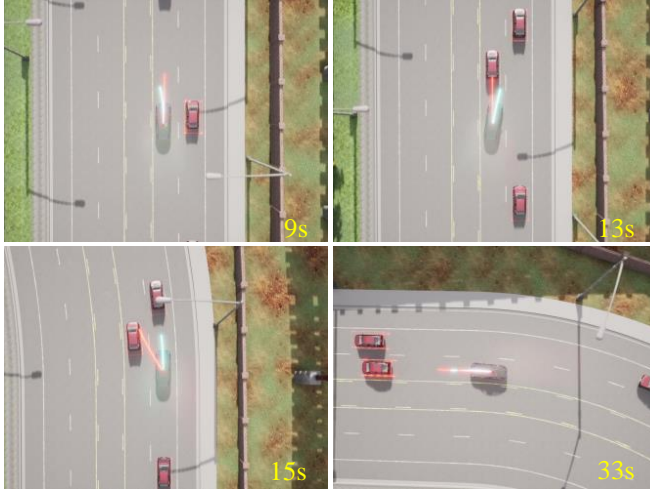
B. Overall Performance

In the implementation of the proposed integrated decision-making and control framework, we first search for a global reference path using A* according to the initial and goal positions, and then obtain the reference trajectory purely based on the global path and current velocity. The prediction horizon is set as $N = 10$ and the sampling time is set as $\Delta T = 0.05$ s.

In each scenario, we select four key frames for visualization from one trial shown in Fig. 2, with their tracking error shown in Fig. 3(a)-(c) respectively. In Scenario 1, as shown in Fig. 2(a), the EV aims to get through the roundabout by following the reference represented by the red ray. The EV is commanded to change its lane to enter/exit the roundabout at 9 s and 18 s. However, the planned path is blocked by the vehicles in front of it. Thus, the EV keeps finding an appropriate chance to change lane, which makes the curve of Δv fluctuates violently. For Scenario 2, as shown in Fig. 2(b), the EV is desired to maintain a speed at 40 km/h. In this trial, the leading vehicle slows down at 9 s, so that the EV merges into its neighbor lane temporarily at 13 s in order to maintain the desired forward velocity; and return to the



(a) Roundabout



(b) Multi-lane Adaptive Cruise Control



(c) Crossroad

Fig. 2. Simulation on three illustrative urban driving scenarios in CARLA. Four key frames are selected for each scenario, and the velocity reference is set to 35 km/h, 40 km/h, 20 km/h, respectively, for the three scenarios from left to right. The red line on the EV represents the trajectory generated from the spline interpolation described in Section II-C while the cyan line shows the optimized predicted trajectory with receding horizon $N = 10$.

TABLE II
OVERALL PERFORMANCE IN DYNAMIC URBAN DRIVING SIMULATION

Scenarios	Succ. Rate (%)	Average Tracking Error			Computation Time (ms)	
		Δp (m)	Δv (m/s)	$\Delta \phi$ (rad)	Ave. \pm SD	Max
Roundabout	93.3	0.495	2.340	0.020	9.39 ± 3.40	24.09
Multi-lane ACC	84.0	0.468	1.742	0.031	11.00 ± 3.41	48.40
Crossroad	80.0	0.424	1.640	0.022	6.86 ± 2.38	30.08

original lane at 15 s to lower the tracking error. In terms of Scenario 3, at the crossroad, the reference speed for the EV is set as 20 km/h. As shown in Fig. 2(c), the EV stops smoothly at the crossroad after the traffic light turns red at 3 s, which leads to the gradually increased velocity error around $t = 5$ s. The peak velocity error at 11 s is caused by the sudden acceleration of the two surrounding vehicles at the intersection.

To further demonstrate the effectiveness of our proposed integrated decision-making and control scheme, we execute the simulation of 30 trials for each scenario and evaluate the performance quantitatively. We define a trial without any vehicle collision as a success. The success rate, computation time together with the average tracking error are listed in Table II. Therefore, our proposed method can be applied to the three highly dynamic scenarios with a satisfactory success rate and good tracking performance. In particular, we achieve the highest success rate in the roundabout scenario at 93.3%. As for the tracking performance, the velocity term is the most significant tracking error among the three scenarios due to the difficulty of maintaining a constant speed in the highly dynamic environment with unpredictable traffic elements, which is consistent with our analysis before on one trail from Fig. 3(a). Yet we can still attain a velocity error lower than 2.3404 m/s in the challenging scenarios. Moreover, the formulated OCP can be solved within milliseconds, from which the real-time performance of the integrated decision-making and control scheme is demonstrated.

With the above analysis, we conclude that the proposed urban autonomous driving framework is able to generate safe reactions, and keep high traffic efficiency with high-level decision-making in real-time with flexible maneuvers.

C. Effectiveness Analysis of the Designed APF

In this section, the effectiveness of the embodied APF in the proposed integrated framework is evaluated. Observed from Fig. 3(d)-(f), the four PFs from vehicles F_V , from traversable lane markings F_{NR} , from non-traversable lane markings F_{CR} , and from traffic lights F_{TL} effected very well. Their combined effect allows the EV to drive reactively, smoothly, and safely to its destination in all three scenarios in Fig. 2. To ensure traffic safety and avoid collision with other vehicles, the vehicle PF should emit repulsive force to the EV when it gets closer to the surrounding ones. But if a surrounding vehicle gets too close, it could generate a relatively large repulsive force on the EV, and the EV will diverge from the target lane. So exerting a repulsive force from the lane marking is necessary to urge the EV to drive in its own lane, so that the traffic rule would be

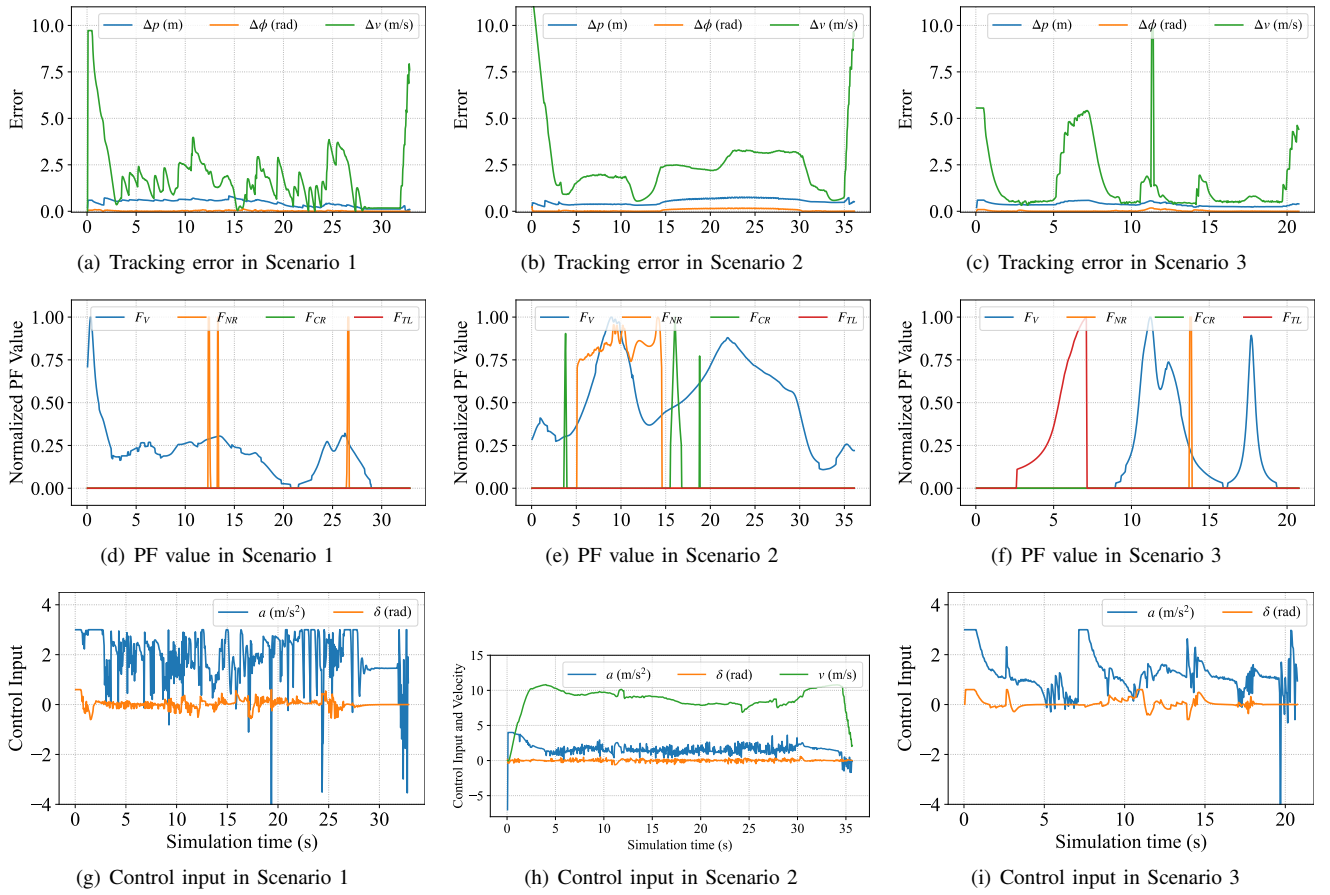


Fig. 3. Tracking error, PF value, and control input from one trail in three urban driving scenarios. (a), (b), (c) record the position error Δp , steering angle error $\Delta \phi$, and target velocity tracking error; (d), (e), (f) record the PF values including $\sum F_V$, $\sum F_{NR}$, $\sum F_{CR}$, and $\sum F_{TL}$; (g), (h), (i) record the acceleration a and steering angle δ .

obeyed by not crossing non-traversable lane markings. In Fig. 2(a), when the EV is exiting the roundabout before 25 s, a surrounding vehicle is driving very closely, and it doesn't mean to exit the roundabout. At this moment, the repulsive force F_V is increasing and urges the EV to leave that vehicle. But as shown in Fig. 3(d), when EV gets closer to the road boundary, there exists a non-traversable lane marking, the repulsive force F_{NR} gets larger rapidly and urged the control output δ keep around 0, which avoids the EV from traversing the road boundary. Thus, it ensures the safety of the EV and prevents traffic rule violations.

Besides, the EV needs to keep in the middle of a strange lane, when it is urged to change lane caused by some vehicles ahead occupying its original lane, like the situation shown in Fig. 2(b) around 13 s. In the multi-lane adaptive cruise control (ACC) simulation trial shown in Fig. 2(b), the EV is cruising on the highway at a given lane but the vehicle ahead blocks its way when $t = 13$ s. Because of the large F_V , the EV changes to its right lane and stays in the middle autonomously with the help of the increasing F_{CR} shown in Fig. 3(e).

To obey the rules regarding dynamic traffic lights in the crossroad scenario in Fig. 2(c), the repulsive force F_{TL} increased smoothly but still quickly when the traffic light

is getting *red*, which causes the EV to stop smoothly and provide a comfortable ride experience. Fig. 3(i) illustrates that when the traffic light becomes red from 3 s to 7 s, the acceleration a became relatively large to brake the EV before the stop line.

In summary, the PF takes effective and urges the control input change reactively with PF values, when different urban driving situations are encountered.

D. Failure Case Analysis

To improve the success rate and enhance the urban driving safety of our proposed integrated decision-making and control scheme, the failure cases in Section IV-B are analyzed in detail. As shown in Table III, collision failure occurs most frequently in the crossroad scenario. Traffic rule violation includes driving to a solid line marking and running a red light, which occurs in the roundabout and multi-lane ACC. Remarkably, vehicles coming from sideways and aggressive overtaking are the two most common accident causes.

1) *Collision with Surrounding Vehicles*: As shown in Fig. 4(a) and Fig. 4(b), the EV encounters surrounding vehicles from the sideways and collides at an almost perpendicular angle. In Fig. 4(c), the EV overtakes the vehicle on the left aggressively and crashed it. One possible reason is that the

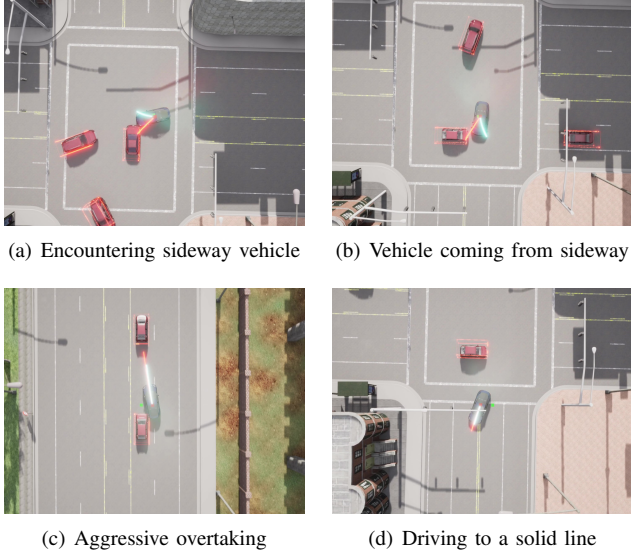


Fig. 4. Typical failure cases in the total 90 trials of simulation in CARLA.

TABLE III
FAILURE CASE CLASSIFICATION AND THEIR FAILURE RATE

Scenarios	Collision rate (%)	Traffic Rule Violation (%)
Roundabout	6.7	6.7
Multi-lane ACC	16.0	6.7
Crossroad	20.0	3.3

prediction of other vehicles' trajectory is naive and the EV doesn't expect the surrounding vehicle to be so aggressive.

2) *Traffic Rule Violation*: In Fig. 4(d), the EV drives onto the solid yellow line, because of avoiding the vehicle on the right. One possible reason is that the PFs for lane markings are not in effect, because there is no explicit lane marking in the crossroad.

V. CONCLUSIONS

In this work, we propose an integrated decision-making and control scheme for urban autonomous driving, in which we encode collision avoidance as well as the compliance with common traffic rules as soft constraints of MPC with the designed PFs in a unified way. High-level decision-making is achieved with simultaneously low-level control with the design of PFs. We implement the proposed framework on three challenging urban driving scenarios, where a high success rate and good tracking performance are attained. Moreover, we demonstrate the effectiveness of the designed PFs in generating safe and flexible maneuvers. From the analysis of several failure cases, our future work is to consider the trajectory prediction of the surrounding vehicles and develop guiding PFs in special areas where explicit traffic regulations are not available.

REFERENCES

- [1] A. Prakash, K. Chitta, and A. Geiger, "Multi-modal fusion transformer for end-to-end autonomous driving," in *Proceedings of the IEEE/CVF Conference on Computer Vision and Pattern Recognition*, 2021, pp. 7077–7087.
- [2] R. Deng, B. Di, and L. Song, "Cooperative collision avoidance for overtaking maneuvers in cellular V2X-based autonomous driving," *IEEE Transactions on Vehicular Technology*, vol. 68, no. 5, pp. 4434–4446, 2019.
- [3] H. Fan, F. Zhu, C. Liu, L. Zhang, L. Zhuang, D. Li, W. Zhu, J. Hu, H. Li, and Q. Kong, "Baidu apollo EM motion planner," *arXiv preprint arXiv:1807.08048*, 2018.
- [4] M. Zhang, N. Li, A. Girard, and I. Kolmanovsky, "A finite state machine based automated driving controller and its stochastic optimization," in *Dynamic Systems and Control Conference*, vol. 58288. American Society of Mechanical Engineers, 2017, p. V002T07A002.
- [5] C. Brewitt, B. Gyevar, S. Garcin, and S. V. Albrecht, "GRIT: Fast, interpretable, and verifiable goal recognition with learned decision trees for autonomous driving," in *2021 IEEE/RSJ International Conference on Intelligent Robots and Systems (IROS)*. IEEE, 2021, pp. 1023–1030.
- [6] C. Xu, W. Zhao, J. Liu, C. Wang, and C. Lv, "An integrated decision-making framework for highway autonomous driving using combined learning and rule-based algorithm," *IEEE Transactions on Vehicular Technology*, vol. 71, no. 4, pp. 3621–3632, 2022.
- [7] F. Gritschneider, P. Hatzelmann, M. Thom, F. Kunz, and K. Dietmayer, "Adaptive learning based on guided exploration for decision making at roundabouts," in *2016 IEEE Intelligent Vehicles Symposium (IV)*. IEEE, 2016, pp. 433–440.
- [8] Z. Zhang, L. Zhang, J. Deng, M. Wang, Z. Wang, and D. Cao, "An enabling trajectory planning scheme for lane change collision avoidance on highways," *IEEE Transactions on Intelligent Vehicles*, 2021.
- [9] J. Chen, B. Yuan, and M. Tomizuka, "Model-free deep reinforcement learning for urban autonomous driving," in *2019 IEEE Intelligent Transportation Systems Conference (ITSC)*. IEEE, 2019, pp. 2765–2771.
- [10] Y. Guan, Y. Ren, Q. Sun, S. E. Li, H. Ma, J. Duan, Y. Dai, and B. Cheng, "Integrated decision and control: toward interpretable and computationally efficient driving intelligence," *IEEE transactions on cybernetics*, vol. 53, no. 2, pp. 859–873, 2022.
- [11] Y. E. Sahin, R. Quirynen, and S. Di Cairano, "Autonomous vehicle decision-making and monitoring based on signal temporal logic and mixed-integer programming," in *2020 American Control Conference (ACC)*. IEEE, 2020, pp. 454–459.
- [12] F. Eiras, M. Hawasly, S. V. Albrecht, and S. Ramamoorthy, "A two-stage optimization-based motion planner for safe urban driving," *IEEE Transactions on Robotics*, vol. 38, no. 2, pp. 822–834, 2021.
- [13] Y. Rasekhipour, A. Khajepour, S.-K. Chen, and B. Litkouhi, "A potential field-based model predictive path-planning controller for autonomous road vehicles," *IEEE Transactions on Intelligent Transportation Systems*, vol. 18, no. 5, pp. 1255–1267, 2016.
- [14] H. Wang, Y. Huang, A. Khajepour, Y. Zhang, Y. Rasekhipour, and D. Cao, "Crash mitigation in motion planning for autonomous vehicles," *IEEE Transactions on Intelligent Transportation Systems*, vol. 20, no. 9, pp. 3313–3323, 2019.
- [15] Y. Ma, P. Zhang, and B. Hu, "Active lane-changing model of vehicle in b-type weaving region based on potential energy field theory," *Physica A: Statistical Mechanics and its Applications*, vol. 535, p. 122291, 2019.
- [16] S. Bae, Y. Kim, J. Guanetti, F. Borrelli, and S. Moura, "Design and implementation of ecological adaptive cruise control for autonomous driving with communication to traffic lights," in *2019 American Control Conference (ACC)*. IEEE, 2019, pp. 4628–4634.
- [17] Q. Ge, Q. Sun, S. E. Li, S. Zheng, W. Wu, and X. Chen, "Numerically stable dynamic bicycle model for discrete-time control," in *2021 IEEE Intelligent Vehicles Symposium Workshops (IV Workshops)*. IEEE, 2021, pp. 128–134.
- [18] T. Weerakoon, K. Ishii, and A. A. F. Nassiraei, "An artificial potential field based mobile robot navigation method to prevent from deadlock," *Journal of Artificial Intelligence and Soft Computing Research*, vol. 5, no. 3, pp. 189–203, 2015.
- [19] J. A. E. Andersson, J. Gillis, G. Horn, J. B. Rawlings, and M. Diehl, "CasADi – A software framework for nonlinear optimization and optimal control," *Mathematical Programming Computation*, vol. 11, no. 1, pp. 1–36, 2019.
- [20] A. Dosovitskiy, G. Ros, F. Codevilla, A. Lopez, and V. Koltun, "CARLA: An open urban driving simulator," in *Conference on Robot Learning*. PMLR, 2017, pp. 1–16.